AGU PUBLICATIONS

Geophysical Research Letters

RESEARCH LETTER
10.1002/2013GL058889

Special Section:
Early Results From the Van Allen Probes

Fine structure of large-amplitude chorus wave packets

O. Santolík[1,2], C. A. Kletzing[3], W. S. Kurth[3], G. B. Hospodarsky[3], and S. R. Bounds[3]

[1]Institute of Atmospheric Physics ASCR, Prague, Czech Republic, [2]Faculty of Mathematics and Physics, Charles University, Prague, Czech Republic, [3]Department of Physics and Astronomy, University of Iowa, Iowa City, Iowa, USA

Key Points:
- Direct 3-D measurements of the magnetic field of intense chorus subpackets
- First detection of variations of the wave vector direction within subpackets
- Wave vector angles are anticorrelated with the logarithm of peak amplitudes

Correspondence to:
O. Santolík,
os@ufa.cas.cz

Citation:
Santolík, O., C. A. Kletzing, W. S. Kurth, G. B. Hospodarsky, and S. R. Bounds (2014), Fine structure of large-amplitude chorus wave packets, *Geophys. Res. Lett.*, *41*, 293–299, doi:10.1002/2013GL058889.

Received 28 NOV 2013
Accepted 13 DEC 2013
Accepted article online 18 DEC 2013
Published online 16 JAN 2014

Abstract Whistler mode chorus waves in the outer Van Allen belt can have consequences for acceleration of relativistic electrons through wave-particle interactions. New multicomponent waveform measurements have been collected by the Van Allen Probes Electric and Magnetic Field Instrument Suite and Integrated Science's Waves instrument. We detect fine structure of chorus elements with peak instantaneous amplitudes of a few hundred picotesla but exceptionally reaching up to 3 nT, i.e., more than 1% of the background magnetic field. The wave vector direction turns by a few tens of degrees within a single chorus element but also within its subpackets. Our analysis of a significant number of subpackets embedded in rising frequency elements shows that amplitudes of their peaks tend to decrease with frequency. The wave vector is quasi-parallel to the background magnetic field for large-amplitude subpackets, while it turns away from this direction when the amplitudes are weaker.

1. Introduction

The role of whistler mode chorus waves in the dynamics of Earth's radiation belts has been demonstrated for both losses [e.g., *Tsurutani et al*., 2009] and local acceleration of relativistic electrons by wave-particle interactions [e.g., *Turner et al*., 2013]. These interactions are usually highly nonlinear [*Summers et al*., 2013]. The frequency-time structure of chorus wave packets is an important parameter for their theoretical analysis [*Tao et al*., 2013]. A fine structure of chorus wave packets has been discovered using the electric field measurements of the Wide Band Data instrument onboard the Cluster mission [*Santolík et al*., 2003a, 2004]. In the equatorial source region of chorus, subpackets have been found to be embedded in the time-frequency structure of chorus elements. They have been observed with a wide range of amplitudes up to more than 30 mV/m at time scales of less than 40 ms. These time scales are an order of magnitude lower than the duration of a chorus element.

Data from other spacecraft missions (STEREO, Time History of Events and Macroscale Interactions during Substorms, and Wind) have subsequently revealed that whistler mode waves with electric fields up to a few hundred mV/m can exist in the inner magnetosphere [*Cattell et al*., 2008; *Cully et al*., 2008; *Kellogg et al*., 2011] although their properties sometimes show distinct differences from chorus. *Wilson et al*. [2011] reported single-component measurements of fluctuating magnetic fields with amplitudes of 4 nT but were unable to determine whether the time-frequency structures were physical or artificial. Their other cases again did not show features consistent with typical properties of whistler mode chorus. *Kurita et al*. [2012] showed vector measurements of magnetic field of several well-resolved chorus elements with amplitudes up to a few hundreds of picotesla but did not analyze their subpacket structure. Full characterization of the wave magnetic field of chorus subpackets which is a crucial parameter for theoretical studies [e.g., *Omura and Nunn*, 2011; *Summers et al*., 2013] has not been obtained up to now.

Chorus is usually assumed to propagate with the wave vector parallel to the background magnetic field in theoretical studies of its generation [*Omura and Nunn*, 2011; *Katoh and Omura*, 2013; *Summers et al*., 2013] and in simulation studies of its interactions with energetic electrons [*Tao et al*., 2013]. Although this assumption seems to correspond well to statistical results based on time averaged data [e.g., *Li et al*., 2013] and to results of case studies of individual chorus elements [e.g., *Kurita et al*., 2012], wave vectors of chorus have also been found close to the whistler mode resonance cone in the equatorial source region [e.g., *Santolík et al*., 2009]. There are currently no data on possible changes of the wave vector directions at time scales of the subpacket structure.

Investigation of whistler mode waves in the outer Van Allen radiation belt is one of the goals of the Electric and Magnetic Field Instrument Suite and Integrated Science (EMFISIS) suite onboard both Van Allen Probes

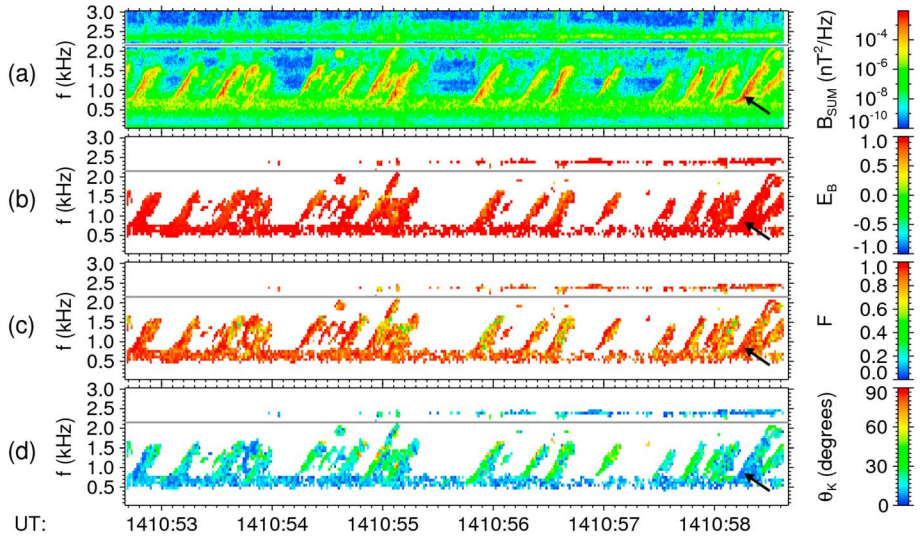

Figure 1. Analysis of one snapshot of magnetic field waveforms recorded by the EMFISIS Waves instrument onboard Van Allen Probe A on 14 November 2012. Frequency-time plots of (a) the sum of the power spectral densities of three orthogonal magnetic components, (b) the ellipticity of the magnetic field polarization with a sign corresponding to the sense of polarization, (c) the planarity of the magnetic field polarization, and (d) the angle between the wave vector and the background magnetic field. A color scale is given on the right-hand side of each plot. Values in Figures 1b–1d are plotted only for power spectral densities above 10^{-6} nT^2 Hz^{-1}. Black arrows point to the time and frequency where the peak of a selected chorus element is detected in Figure 2. One half of the local electron cyclotron frequency is given by a grey line in each plot. Time is given in UT at the bottom.

spacecraft. In this letter, we show the first results of new multicomponent waveform measurements of whistler mode chorus subpackets recorded by the EMFISIS Waves instrument. We present data on their instantaneous peak amplitudes directly measured by three-axial magnetic search coils. We also analyze the first measurements of variations of the wave vector directions at the time scales of chorus substructure. Our letter gives initial answers to the following questions: (1) How large are the local magnetic field maxima within intense chorus elements, and how are they linked to the wave frequency? (2) Does the wave vector direction vary during the nonlinear generation process of intense chorus wave packets? (3) Are the instantaneous wave vector directions correlated with the amplitudes of magnetic field subpackets?

2. The EMFISIS Continuous Waveform Burst Mode Data

The EMFISIS instrument suite is carried by Van Allen Probes spacecraft to measure the background magnetic fields by a triaxial fluxgate magnetometer and wave magnetic field fluctuations by a triaxial search coil magnetometer. A comprehensive set of wave electric and magnetic field measurements is processed by the EMFISIS Waves instrument which also uses external signals from the Electric Fields and Waves experiment. Six inputs from sensors making 3-D measurements of both the electric and the magnetic field are detected by six identical waveform receivers with a flat (to within 1 dB) response from 10 Hz to 12 kHz. The phase-matched waveforms are digitized at a sampling rate of 35 kHz with a 16 bit instantaneous dynamic range (see *Kletzing et al.* [2013] for a complete description). In the present case study we concentrate our attention on 3-D magnetic field waveforms which have been captured in a continuous waveform burst mode. This mode provides us with selected 5.968 s snapshots of data from search coil magnetometers.

Figure 1 shows an example of a simple spectral analysis of one snapshot of 3-D magnetic field waveforms recorded onboard Van Allen Probe A on 14 November 2012 after 14:10:52.680 UT. The observations were made in the outer Van Allen belt at a radial distance (R) of 5.3 Earth radii, in the equatorial source region of chorus at a magnetic dipole latitude (λ_m) of −2.4°, and in the morning sector at a magnetic local time (MLT) of 6.9 h. An overlapped (70%) 1024-point Fast Fourier Transform is used to obtain complex spectra of each component and to form averaged spectral matrices with a time resolution of 18 ms and with a frequency resolution of 68 Hz. The traces of the spectral matrices correspond to magnetic power spectral densities shown in Figure 1a. We can notice a sequence of rising frequency chorus elements in the lower band below

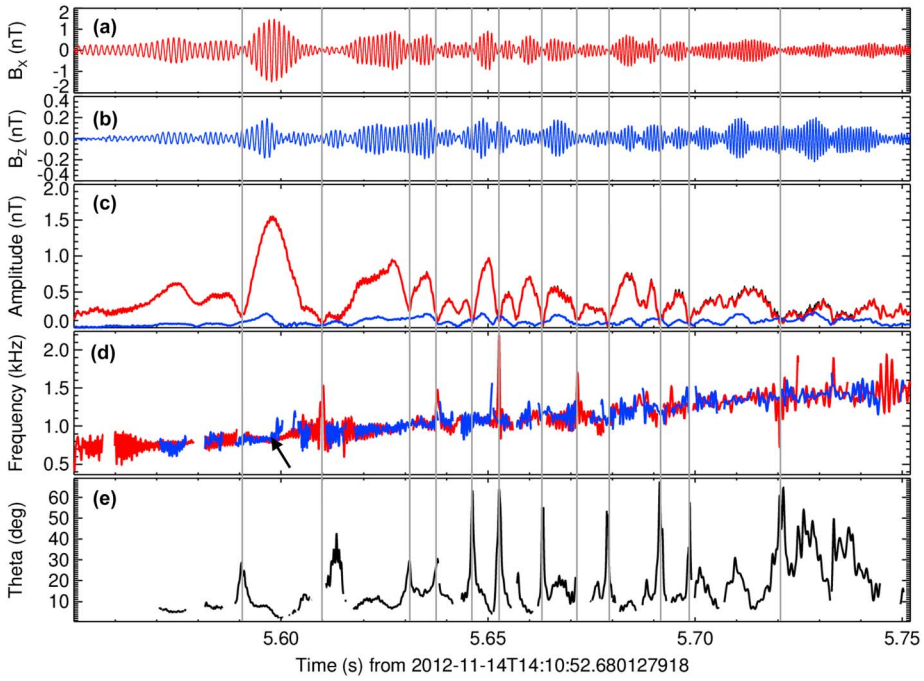

Figure 2. Detailed analysis of a single chorus element marked by an arrow in Figure 1 and observed on 14 November 2012 after 14:10:52.680. (a) Measured waveform of a magnetic field component B_X perpendicular to $\boldsymbol{B}_0$. (b) Waveform of the component B_Z parallel to $\boldsymbol{B}_0$. (c) Instantaneous amplitudes of these two waveforms, a red line shows A_X, and a blue line shows A_Z; a black line which is often hidden behind the A_X results corresponds to instantaneous total magnetic field B. (d) Instantaneous frequency with the same color coding as in Figures 2a and 2b; the results are plotted only when the instantaneous amplitude of the corresponding component is $>$ 50 pT; a black arrow points to the same time and frequency of the maximum amplitude as in Figure 1. (e) Instantaneous angle between the wave vector and $\boldsymbol{B}_0$; the results are plotted only when the instantaneous amplitudes of all the magnetic field components are $>$ 50 pT. Vertical grey lines should guide the eye through all the panels by showing selected minima of A_X.

one half of the electron cyclotron frequency (i.e., below 2.16 kHz, in this case). The ellipticity and planarity, and the angle θ_K between the wave vector and $\boldsymbol{B}_0$ (Figures 1b–1d, respectively) have been obtained from the singular value decomposition of the magnetic spectral matrices [*Santolík et al.*, 2003b]. The results show nearly circularly, right-hand polarized whistler mode chorus waves, with the magnetic field polarization confined close to a single plane. The estimated normal direction to this plane shows that the waves are often propagating quasi-parallel to the background field at θ_K below 30° but sometimes also at higher angles around 60°.

3. Instantaneous Amplitudes, Frequencies, and Wave Vector Directions

A black arrow plotted before the end of the time interval in Figure 1 indicates the time and frequency of the peak of a strong chorus element which is shown in detail in Figure 2 using the high-resolution waveform measurements. The measured waveforms are first calibrated using a frequency-dependent transfer function of the sensor-receiver chain. The results are then transformed from the spinning spacecraft system to a system which is fixed with respect to the sunward direction and linked to the locally measured background magnetic field $\boldsymbol{B}_0$. For this transformation, we use the fluxgate magnetometer data averaged to the time resolution of 94 ms (which corresponds to an angular resolution of ~3° in the spin plane). Figures 2a and 2b indicate that the component parallel to $\boldsymbol{B}_0$ (B_Z) is much smaller than one of the components perpendicular to $\boldsymbol{B}_0$ (B_X) which reaches an amplitude of 1.5 nT (1% of the background magnetic field). We can also notice the fine structure of wave packets which are different in the two components. The other component perpendicular to $\boldsymbol{B}_0$ (B_Y, not shown) has very similar amplitudes as B_X. To analyze the behavior of instantaneous wave amplitudes and phases, we have separately pass band filtered each of the components between 0.4 and 3 kHz and performed the Hilbert transform. The result is a complex analytical signal whose amplitude is plotted in Figure 2c for B_Z (blue) and B_X (red). The instantaneous total magnetic field, $B = \sqrt{B_X^2 + B_Y^2 + B_Z^2}$, is

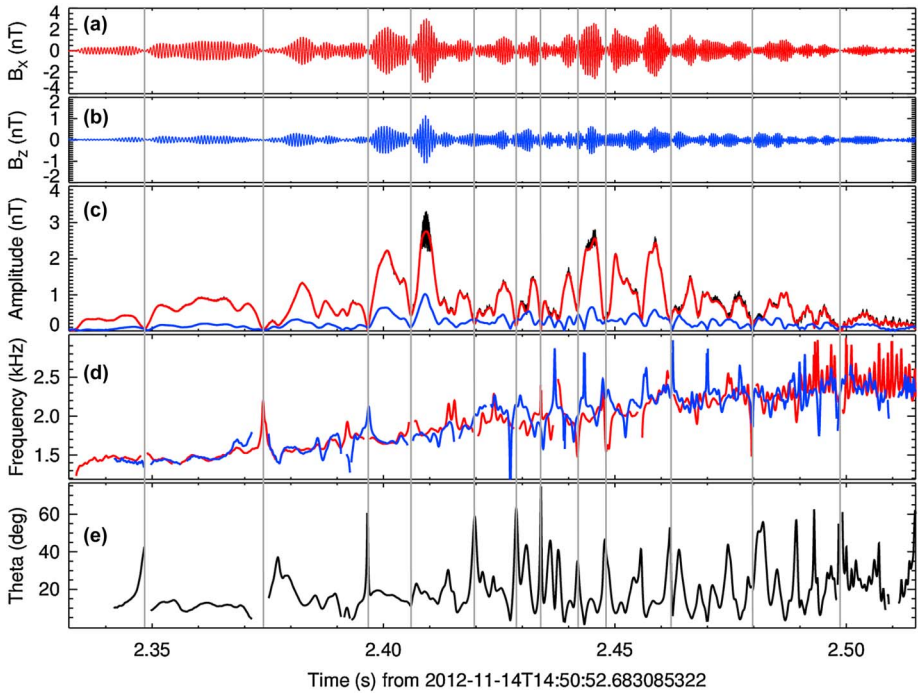

Figure 3. The same as in Figure 2 but for another chorus element observed by the EMFISIS Waves instrument onboard Van Allen Probe A on 14 November 2012 after 14:50:52.683.

represented by a black line which is most of the time hidden behind the red line of the B_X amplitude. The time derivative of the phase of the complex analytic signal gives the instantaneous frequency which is plotted in Figure 2d using the same red and blue color coding. The chorus element, rising in frequency from 600 Hz to 1.5 kHz, is clearly seen in both components, with fluctuations corresponding to uncertainties of the analysis. Figure 2e shows the instantaneous angle between the wave vector and $\boldsymbol{B}_0$. Its value is obtained by the same method as in Figure 1d from a spectral matrix, $S_{kl} = A_k A_l \, e^{i(\varphi_k - \varphi_l)}$, where $i = \sqrt{-1}$, $k = x, y, z$; $l = x, y, z$; φ_k, and φ_l are instantaneous phases; and A_k and A_l are instantaneous amplitudes. The results show that the wave vector angle can change by tens of degrees within a single chorus subpacket. However, this angle is generally below 30° at the local maxima of the instantaneous total magnetic field, with an exception of the final part of the chorus element (at frequencies above 1.2 kHz) where we observe higher angles. All these variations visibly correspond to the ratio of amplitudes of the B_Z and B_X waveforms seen in Figures 2a–2c. The wave vector angle is small for low B_Z and high B_X amplitudes, and it starts to grow whenever the B_X amplitudes decrease.

Figure 3 shows results of the same analysis for another selected chorus element from a different snapshot of the EMFISIS continuous waveform burst mode data. The snapshot was taken onboard Van Allen Probe A on 14 November 2012, after 14:50:52.683 UT, at $R = 4.7$ Earth radii, $\lambda_m = -2.6°$, and MLT = 7.5 h. The spacecraft is therefore still located in the equatorial source region of chorus and in the morning sector but slightly closer to the Earth than in the previous example. A rising frequency chorus element is found at higher frequencies (Figure 3d), but it still stays in the lower band of chorus below one half of the locally measured electron cyclotron frequency ($f_{ce}/2$–2.95 kHz). A structure of subpackets is detected in the 3-D waveforms (Figures 3a and 3b), with similar properties as in the previous case but at higher peak instantaneous amplitudes up to ~3 nT (1.4% of the background field). The instantaneous total field B is fluctuating around this value in the peaks (Figure 3c, black line). This effect results from a minor digital clipping of the highest observed signals seen for a few wave periods in the raw data (not shown) from the separate search coil sensors. The wave vector angle (Figure 3e) again changes by tens of degrees within some of the subpackets, but it generally stays below 30° at the local maxima of the instantaneous amplitudes. Note that the observed minor waveform clipping can only lead to an underestimation of the dominant magnetic field components perpendicular to $\boldsymbol{B}_0$ and therefore to a slight overestimation of the wave vector angle at the highest peaks.

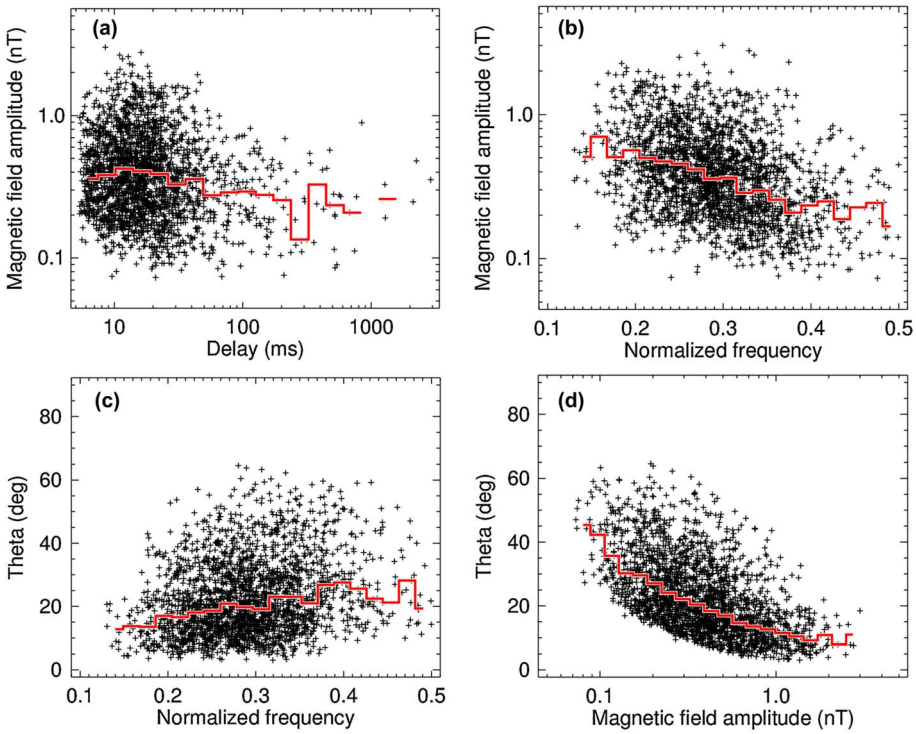

Figure 4. Results of a systematic analysis of 2230 subpackets of whistler mode chorus collected by the Van Allen Probes A spacecraft in the equatorial morningside region at $R \sim 5$ Earth radii on 14 November 2012 between 12:00 and 15:00 UT. (a) Magnetic field amplitudes at subpacket peaks as a function of the time delay between neighboring subpacket peaks; (b) magnetic field amplitude at subpacket peaks and (c) instantaneous angle between the wave vector and $\boldsymbol{B}_0$, both as a function of the wave frequency normalized by the locally measured electron cyclotron frequency; (d) instantaneous angle between the wave vector and $\boldsymbol{B}_0$ as a function of the magnetic field amplitude at subpacket peaks. Median values are calculated in 20 regularly spaced abscissa intervals and plotted by a red line in each plot.

4. Systematic Analysis Based on a Large Number of Subpackets

The examples in Figures 2 and 3 indicate that the instantaneous amplitudes and wave vector angles may be interdependent. Additionally, they both may depend on instantaneous frequency. We have therefore analyzed a large number of chorus subpackets recorded within 3 h on 14 November 2012, between 12:00 and 15:00 UT. During this time interval, the Van Allen Probe A spacecraft moved along its orbit on the morningside of the equatorial magnetosphere between $R = 5.7$ and $R = 4.6$ Earth radii, λ_m from $-0.4°$ to $-2.6°$, and MLT from 5.4 h to 7.6 h. The EMFISIS onboard data selection algorithm was aimed at strong chorus events. It was based on the integrated power obtained from the three-axial magnetic field search coils in the frequency range between 0.1 and 0.7 $f_{ce.}$ During the analyzed 3 h time interval, 45 strongest snapshots of 3-D waveforms were selected and recorded. Duration of each of them was the same as for the example shown in Figure 1, i.e., 5.968 s. In all 45 snapshots, the three magnetic field components have been analyzed to obtain instantaneous amplitudes, frequencies, and wave vector directions by the method described in the previous section.

We have then searched the data of instantaneous amplitudes of the B_X component for local maxima (peaks). To distinguish the chorus wave packets from the weaker background hiss we have set a lower threshold for the local maxima: the peaks have to be at least 50 pT above both adjacent minima. For the analyzed frequency band (0.4–3 kHz), this threshold corresponds to the lower limit of power spectral densities at 10^{-6} nT^2 Hz^{-1} which has been used to distinguish chorus elements in Figure 1. Note that this limit is well above the integrated sensor noise (0.3 pT) in the same frequency band. Another obvious criterion which has been used to define the local maxima of instantaneous amplitudes is that they must be at least one wave period of the lowest analyzed frequency (400 Hz) apart from both adjacent minima.

From the resulting list of the B_X local maxima we have removed all the cases where the instantaneous frequency for any of the other two components differed by more than 10% from the instantaneous frequency of the B_X component. To stay within the lower band of chorus, we have also removed all the cases where the instantaneous

frequency was above one half of the locally measured electron cyclotron frequency. For the resulting set of 2230 subpacket peaks, the characteristic total magnetic field was estimated as a median value of B in an interval of one instantaneous wave period around each peak.

The results are plotted in Figure 4a as a function of the time delay between neighboring subpacket peaks, following a similar format as in *Santolík et al.* [2004, Figure 5]. We can notice that most of the delays in our case occur between 5 ms (a lower limit imposed by our analysis) and a few tens of milliseconds. These delays correspond to the fine structure of chorus subpackets embedded inside chorus elements. Larger delays occur less frequently, reflecting intervals between the separate chorus elements. The corresponding B amplitudes at the subpacket peaks vary in a broad interval from several tens of picotesla (a lower limit imposed by the analysis method) up to a few nanotesla, with no clear dependence on the delays. The median subpacket B amplitudes in 20 intervals of delays reach values between 200 and 400 pT, while the median of all the amplitudes is 367 pT.

The magnetic field amplitudes as a function of the normalized wave frequency are shown in Figure 4b. The frequency normalization factor is the electron cyclotron frequency f_{ce} obtained from the locally measured background magnetic field. The peaks of the subpackets are found at frequencies from 0.14 f_{ce} to 0.49 f_{ce}, but most often, they occur between 0.2 f_{ce} and 0.4 f_{ce}. Although the corresponding amplitudes are again significantly spread, we can notice that higher normalized frequencies usually imply lower amplitudes. The median subpacket amplitudes in 20 intervals of normalized frequencies decrease from ~700 pT down to ~200 pT. On the other hand, the instantaneous angle between the wave vector and $\boldsymbol{B}_0$ shows an opposite behavior in the same interval of normalized frequencies (Figure 4c). Its median values increase from ~15° to ~30°, but the waves at the individual subpacket peaks propagate in a large interval of wave vector angles from a few degrees up to more than 60°.

A question therefore arises whether the observed values of subpacket amplitudes and corresponding wave vector angles are interdependent or not. Figure 4d gives a clear answer: The instantaneous wave vector angles at subpacket maxima are anticorrelated with the logarithm of their corresponding magnetic field amplitudes. Not only the median values of the wave vector angles show an approximately exponential decrease from ~40° (at amplitudes below 100 pT) down to ~10° (at amplitudes above 1 nT) but also the spread of the obtained points is considerably lower than in Figures 4a–4c. For strong amplitudes ($>$1 nT), all the obtained wave vector angles are found below 35°. Additionally, the wave vector angles seem to obey an amplitude-dependent lower cutoff of their values, at ~25° for 100 pT and below ~5° at amplitudes larger than 1 nT.

5. Discussion

New data of the Van Allen Probes EMFISIS instrument allow us to directly measure magnetic field components of whistler mode chorus and their polarization at time scales of the fine structure of wave subpackets. Our case study of morningside chorus in the outer radiation belt concentrates on analysis of sequences of subpackets embedded in rising frequency lower band chorus elements observed in the equatorial region. The time delays between the neighboring subpacket maxima have been found between several milliseconds and several tens of milliseconds, consistent with the previously published results of the Cluster mission [*Santolík et al.*, 2003a, 2004].

At peaks of the subpackets the magnetic field amplitudes vary in a broad interval from the lower limit imposed by our analysis method (several tens of picotesla) up to 3 nT, i.e., more than 1% of the background magnetic field. The peak amplitudes tend to decrease with frequency throughout the range of the lower band of chorus although the spread of obtained values is significant. The median of all the obtained subpacket peak amplitudes is ~370 pT. These values are consistent with a possible nonlinear generation mechanism of the fine structure of chorus related to the threshold amplitude for the nonlinear wave growth [*Omura et al.*, 2009; *Omura and Nunn*, 2011; *Kurita et al.*, 2012; *Summers et al.*, 2013]. These large magnetic field amplitudes of chorus subpackets would also induce nonlinear interactions and possible acceleration of radiation belt electrons to relativistic energies [*Tao et al.*, 2013]. Note, however, that the importance of this process has yet to be determined; both the onboard data selection algorithm and our analysis method may lead to a bias toward larger peak values, while lower peak values are most probably under represented.

Instantaneous wave vector directions have been determined for the first time at time scales of the fine structure of chorus subpackets. Our results reveal that instantaneous wave vector directions can change by tens of degrees within a single chorus subpacket. They can also vary throughout the entire time-frequency

structure of a chorus element. Although the fine structure of chorus subpackets has already been taken into account by *Tao et al.* [2013] in their analysis of nonlinear effects of chorus on radiation belt electrons, our discovery of variations of instantaneous wave vector directions might represent a new aspect in these studies. We have furthermore found that the instantaneous wave vector angles at subpacket maxima are anticorrelated with the logarithm of their corresponding magnetic field amplitudes. The wave vectors are quasi-parallel to the background magnetic field for large-amplitude subpackets, while they turn away from the quasi-parallel direction when the amplitudes are weaker. The spread of the obtained points is considerably lower than in the cases of separate analysis of amplitudes and wave vector angles as a function of frequency. The wave vector angles additionally seem to obey an amplitude-dependent lower cutoff of their values.

This observation might be hypothetically linked to properties of the whistler mode waves which, at large wave vector angles, tend to decrease the ratio of the magnetic field power to the electric field power. However, linear cold plasma theory shows that significant effects can be expected only very close to the whistler mode resonance angle [e.g., *Santolík et al.*, 2009]. This is not consistent with our observations because we obtain a significant decrease of median magnetic field amplitudes even for small inclinations of the wave vector from the parallel direction. A possible explanation of this effect might be that wave vector directions change during the generation process to fulfill the resonance condition, but the parallel wave vectors are generated with larger amplitudes. This would be the case for the linear cyclotron instability, related to the electron temperature anisotropy observed in the equatorial region [*Kurita et al.*, 2012]. Taking into account that a nonlinear generation mechanism most probably plays a significant role in this process, our results may challenge the current theoretical understanding of the origin of chorus which does not take into account the fine structure of subpackets.

Acknowledgments

We acknowledge the hard work of the entire Van Allen Probes EMFISIS team on the instrument design, testing, calibration, and operations. We would also like to thank the EFW team for supporting cross calibration of the two sets of instruments. This work was supported from JHU/APL contract 921647 under NASA Prime contract NAS5-01072. O. Santolík acknowledges support from GACR grant 205-10-2279, LH11122, and EU support through the FP7-Space grant agreement 284520 for the MAARBLE collaborative research project.

The Editor thanks two anonymous reviewers for their assistance in evaluating this manuscript.

References

Cattell, C., et al. (2008), Discovery of very large amplitude whistler-mode waves in Earth's radiation belts, *Geophys. Res. Lett.*, *35*, L01105, doi:10.1029/2007GL032009.

Cully, C. M., J. W. Bonnell, and R. E. Ergun (2008), THEMIS observations of long-lived regions of large-amplitude whistler waves in the inner magnetosphere, *Geophys. Res. Lett.*, *35*, L17S16, doi:10.1029/2008GL033643.

Katoh, Y., and Y. Omura (2013), Effect of the background magnetic field inhomogeneity on generation processes of whistler-mode chorus and broadband hiss-like emissions, *J. Geophys. Res. Space Physics*, *118*, 4189–4198, doi:10.1002/jgra.50395.

Kellogg, P. J., C. A. Cattell, K. Goetz, S. J. Monson, and L. B. Wilson III (2011), Large amplitude whistlers in the magnetosphere observed with Wind-Waves, *J. Geophys. Res.*, *116*, A09224, doi:10.1029/2010JA015919.

Kletzing, C. A., et al. (2013), The Electric and Magnetic Field Instrument Suite and Integrated Science (EMFISIS) on RBSP, *Space Sci. Rev.*, *179*, 127–181, doi:10.1007/s11214-013-9993-6.

Kurita, S., Y. Katoh, Y. Omura, V. Angelopoulos, C. M. Cully, O. Le Contel, and H. Misawa (2012), THEMIS observation of chorus elements without a gap at half the gyrofrequency, *J. Geophys. Res.*, *117*, A11223, doi:10.1029/2012JA018076.

Li, W., J. Bortnik, R. M. Thorne, C. M. Cully, L. Chen, V. Angelopoulos, Y. Nishimura, J. B. Tao, J. W. Bonnell, and O. LeContel (2013), Characteristics of the Poynting flux and wave normal vectors of whistler-mode waves observed on THEMIS, *J. Geophys. Res. Space Physics*, *118*, 1461–1471, doi:10.1002/jgra.50176.

Omura, Y., and D. Nunn (2011), Triggering process of whistler mode chorus emissions in the magnetosphere, *J. Geophys. Res.*, *116*, A05205, doi:10.1029/2010JA016280.

Omura, Y., M. Hikishima, Y. Katoh, D. Summers, and S. Yagitani (2009), Nonlinear mechanisms of lower-band and upper-band VLF chorus emissions in the magnetosphere, *J. Geophys. Res.*, *114*, A07217, doi:10.1029/2009JA014206.

Santolík, O., D. A. Gurnett, J. S. Pickett, M. Parrot, and N. Cornilleau- Wehrlin (2003a), Spatio-temporal structure of storm-time chorus, *J. Geophys. Res.*, *108*(A7), 1278, doi:10.1029/2002JA009791.

Santolík, O., M. Parrot, and F. Lefeuvre (2003b), Singular value decomposition methods for wave propagation analysis, *Radio Sci. 38*(1), 1010, doi:10.1029/2000RS002523.

Santolík, O., D. A. Gurnett, J. S. Pickett, M. Parrot, and N. Cornilleau-Wehrlin (2004), A microscopic and nanoscopic view of storm-time chorus on 31 March 2001, *Geophys. Res. Lett.*, *31*, L02801, doi:10.1029/2003GL018757.

Santolík, O., D. A. Gurnett, J. S. Pickett, J. Chum, and N. Cornilleau-Wehrlin (2009), Oblique propagation of whistler mode waves in the chorus source region, *J. Geophys. Res.*, *114*, A00F03, doi:10.1029/2009JA014586.

Summers, D., R. Tang, Y. Omura, and D.-H. Lee (2013), Parameter spaces for linear and nonlinear whistler-mode waves. *Phys. Plasmas*, *20*, 072110, doi:10.1063/1.4816022.

Tao, X., J. Bortnik, J. M. Albert, R. M. Thorne, and W. Li (2013), The importance of amplitude modulation in nonlinear interactions between electrons and large amplitude whistler waves, *J. Atmos. Sol. Terr. Phys.*, *99*, 67–72.

Tsurutani, B. T., O. P. Verkhoglyadova, G. S. Lakhina, and S. Yagitani (2009), Properties of dayside outer zone chorus during HILDCAA events: Loss of energetic electrons, *J. Geophys. Res.*, *114*, A03207, doi:10.1029/2008JA013353.

Turner, D. L., V. Angelopoulos, W. Li, M. D. Hartinger, M. Usanova, I. R. Mann, J. Bortnik, and Y. Shprits (2013), On the storm-time evolution of relativistic electron phase space density in Earth's outer radiation belt, *J. Geophys. Res. Space Physics*, *118*, 2196–2212, doi:10.1002/jgra.50151.

Wilson, L. B., III, C. A. Cattell, P. J. Kellogg, J. R. Wygant, K. Goetz, A. Breneman, and K. Kersten (2011), The properties of large amplitude whistler mode waves in the magnetosphere: Propagation and relationship with geomagnetic activity, *Geophys. Res. Lett.*, *38*, L17107, doi:10.1029/2011GL048671.